Sb surface terminated MnSb devices in the niccolite phase

Cite as: APL Mater. 12, 011107 (2024); doi: 10.1063/5.0181131
Submitted: 14 October 2023 • Accepted: 26 December 2023 •
Published Online: 12 January 2024

S. N. Holmes,[1,a] C. W. Burrows,[2,b] G. R. Bell,[2,c] I. Farrer,[3,d] and D. A. Ritchie[3,e]

AFFILIATIONS

[1] Department of Electronic and Electrical Engineering, University College London, Torrington Place, London WC1E 7JE, United Kingdom
[2] Department of Physics, University of Warwick, Coventry CV4 7AL, United Kingdom
[3] Cavendish Laboratory, University of Cambridge, J. J. Thomson Avenue, Cambridge CB3 0HE, United Kingdom

Note: This paper is part of the Special Topic on Spin-Related Quantum Materials and Devices.
[a] **Author to whom correspondence should be addressed:** stuart.holmes@ucl.ac.uk
[b] **Present address:** Diamond Light Source Ltd., Harwell Science Innovation Campus, Didcot, Oxfordshire, OX11 0DE, U.K. chris.burrows@diamond.ac.uk
[c] gavin.bell@warwick.ac.uk
[d] **Present address:** Department of Electronics and Electrical Engineering, University of Sheffield, Mappin Street, Sheffield. S1 3JD, U.K. i.farrer@sheffield.ac.uk
[e] dar11@cam.ac.uk

ABSTRACT

The magneto-electronic properties of ferromagnetic MnSb grown by molecular beam epitaxy can be dominated by the presence of a surface state in the minority spin bandgap when the surface is Sb-terminated. The material resistivity is 120 $\mu\Omega$.cm at 295 K, and although this is determined by the majority spin population, the anisotropic magnetoresistance, dependent on minority spins, is ~0.24% for the Sb-terminated devices with Mn-terminated devices showing ~0.02%. At 295 K, the extraordinary Hall constant is 0.5 Ω/T for the Sb-terminated surface and 1.5 Ω/T for the Mn-terminated surface with the extraordinary Hall constant and anisotropic magnetoresistance behaving with an anomalous temperature dependence between 295 and 1.5 K. The dominant MnSb structural phase on the GaAs (001) orientation is naturally doped p-type with a carrier density ~1×10^{22} cm^{-3} determined by the normal Hall effect after the extraordinary Hall effect has saturated at higher fields than ~2 T. Spintronic device possibilities are discussed, particularly the spin-light emitting diode and magnetic nano-structures. A natural p-type doping in MnSb limits the devices to dominant hole carrier effects although there is compatibility with both III–V and Si–Ge materials for hybrid device possibilities.

I. INTRODUCTION

Electronic devices with enhanced Topological insulator (TI) properties promise a range of behavior that was not fully understood until a few years ago (see Ref. 1). A model to predict which particular materials show topological behavior can be accessed now (see Refs. 2 and 3), and in the set of materials where TI behavior is predicted, MnSb has a TI surface state in the niccolite-phase (structure $B8_1$) and non-TI behavior in the cubic-phase (structure $B3$). This prediction is not the full story of this material by any means, and we discuss the influence of the MnSb surface termination in the following *Applied Physics Letters Materials* paper. MnSb is a transition metal pnictide semiconductor with ferromagnetic ordering properties that have been applicable to spintronic devices, particularly the spin-light emitting diode (spin-LED) as the p-type, hole spin-injector,[4,5] the MTJ[6] (magnetic tunnel junction), and nano-scaled quantum dots.[7]

Several structural phases of MnSb can be stabilized on GaAs substrates with the cubic-phase already showing half-metallic properties, such as a minority spin band-gap with an integer spin

magnetic moment.[8] Molecular Beam Epitaxy (MBE) growth of MnSb has compatibility with common III-V semiconductors, such as GaAs/InGaAs,[9–11] and also recently growth using InGaSb layers was reported,[12] adding to the attraction of this material for possible hybrid devices.

In this paper, we discuss the magneto-electronic properties of niccolite-phase MnSb (1–101) orientation layers (this is the hexagonal "NiAs" phase $B8_1$) that are grown on n-type GaAs (001) substrates and further outline their device potential considering the presence of minority spin band surface states. Section I is a summary of the device potential of MnSb and an introduction to some of the structural properties. In Sec. II, device fabrication is discussed, and in Sec. III, the magneto-optical and magneto-transport measurements are reported. Section IV is a discussion of the experimental data, and Sec. V is an overall summary of the important points.

Spintronic devices in MnSb have a p-type background conductivity with uses reported for spin-injection into hole-gases from a p-type reservoir for spin transport or for emission from a p–n junction device.[13] A MnSb-based spin-LED device with side emission[4,5] had a 2.1% polarization efficiency at 30 K. This low value is due to the p-type conduction type with (minority) electron injection rather than holes from a Zener tunneling process with high electric fields involved in the device operation. This compares extremely unfavorably with the n-type MnAs spin-LED where the efficiency is 26% at 7 K (see Ref. 14). MnAs can also be used as a spin-injector component with wurtzite-phase GaN showing the compatibility with different material combinations, at least for MnAs.[15] The surface magnetic properties of MnSb are different from the bulk wafer with the vacuum surface dominating the magnetoresistance behavior, Ref. 16 revealed the properties of this surface distinct from the bulk. Nano-scaled MnSb dots showed a modest magnetoresistance of 0.05%–0.1% variation in 1 T applied field[7] with field anisotropy evident. A MTJ showed a 30.5% tunneling spin-polarization at 0.25 K and 2 T (see Ref. 6). Quasi-two-dimensional islands of cubic MnSb are thought to be responsible for the magnetoresistance properties of GaSb/Mn digital alloys and indeed are strongly p-type.[17]

MBE growth predominantly produces a niccolite-phase of MnSb on GaAs (001) with a hexagonal crystal lattice although smaller crystals of zinc blende and wurtzite-phase MnSb can be stabilized[8] with growth on the GaAs (111)B surface. Reference 16 reported that the (1–101) MnSb surface on GaAs (001) was registered with a 32° rotation to the (001) surface. Previous growth studies[18,19] identified the importance of protecting the surface from oxidation with an Sb-termination. Surface reconstruction can be prevalent with a complicated two-phase reconstruction mechanism.[20] The magneto-electronic properties of MnSb are dominated by the surface state that exists in the case of Sb surface-termination, and half-metallic behavior can be preserved at this surface even in the niccolite-phase due to a surface reconstruction.[10] Dirac-fermion states have been predicted in the minority spin bandgap of MnSb-terminated NiMnSb surfaces,[21] and these current carrying states provide a scattering pathway for an anisotropic magnetoresistance at the surface. Figure 1 shows a predicted band structure of reconstructed MnSb-based on the literature referenced so far in this paper.

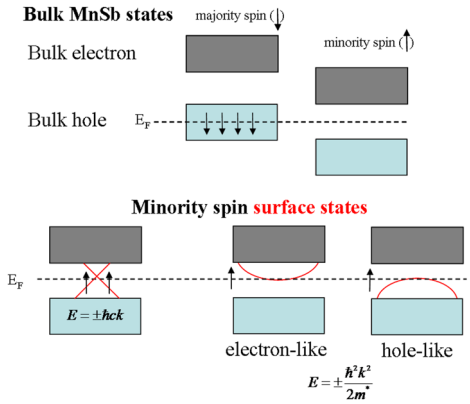

FIG. 1. A schematic of the bulk and surface states at the Sb-terminated surface of niccolite-phase MnSb. E_f is the Fermi level, k is the wave-vector, $\hbar$ is Planck's constant, c is the carrier velocity, and m* is the effective mass. The fundamental energy gap is ~1.08 eV.

II. DEVICE PREPARATION

The MnSb wafers were grown by MBE on n-type GaAs (001) MBE grown wafers. As-capping was used to prevent contamination of the GaAs surface prior to growth of the MnSb. The MnSb growth temperature was 415–420 °C, and the Sb_4/Mn flux ratio was seven. *In situ* RHEED (Reflection high energy electron diffraction) *rod* structure could be seen corresponding to the MnSb (1–101) direction. The MnSb epilayers were either un-capped (in which case naturally MnO/MnO_2-terminated) or intentionally Sb-terminated after cooling in an Sb flux (see Table I for a summary). Crystalline Sb-termination on the surface of wafer G was characterized by RHEED *spots* appearing on the diffraction *rods*, indicative of a three-dimensional growth.

Standard optical lithography, semiconductor device processing was used. The processing temperatures were kept below ~200 °C to avoid oxidation of MnSb. The Hall bar mesa was etched with $HCl:H_2O$ (1:10) stopping selectively at the GaAs surface [see the inset of Fig. 2(c)]. The Hall bar channel was either parallel to

TABLE I. A summary of the MnSb wafers in this study. They were grown with a beam flux ratio (J_{Sb}/J_{Mn}) of seven and a growth temperature between 415 and 422 °C. The As-capped GaAs substrates were desorbed at 420 °C prior to growth of MnSb.

Wafer	t (nm)	ρ ($\mu\Omega$.cm)	Surface termination
A	15	97	No Sb cap
B	45	a	No Sb cap
C	15	130	No Sb cap
D	16	93	Sb-termination and etch test[b]
E	75	100	Polycrystalline-no Sb cap
F	15	170	No Sb cap
G	15	400	Sb-termination

[a] Arbitrary shaped device.
[b] The etch test device had the Sb-surface termination removed with dilute HCl to subsequently re-measure the magneto-electronic properties—see Sec. IV.

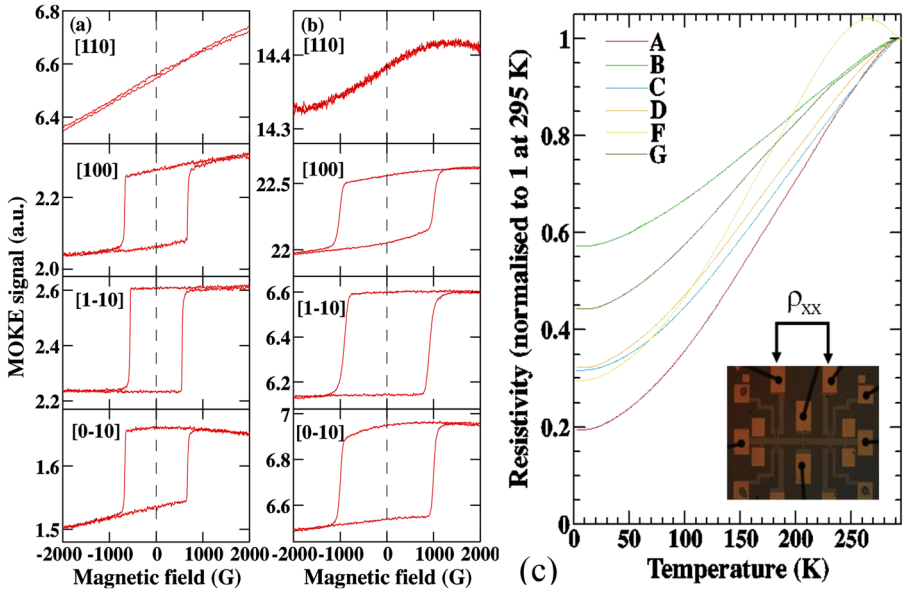

FIG. 2. The longitudinal MOKE signal from (a) device F (no Sb-cap) and (b) device G (Sb-termination) at 295 K, showing the reproducibility of the uniaxial behavior between nominally identical growths. The crystal directions correspond to the GaAs (001) in-plane orientations. (c) Device resistivity on cooling from 295 to 1.7 K. The resistance values are normalized to 1.0 at 295 K. The 295 K resistivity values range from 93 to 400 $\mu\Omega$.cm due to different p-type background densities and levels of disorder. The inset shows an optical image of the Hall bar mesa (wafer C).

the Uniaxial Magnetic Anisotropic (UMA), easy axis (EA), or the UMA HA (Hard axis). Ohmic contacts to the MnSb were made with 100 nm thickness of Ti–Au, and this was confirmed via linear current–voltage characteristics down to 1.7 K. Magnetic nanostructures were also made with electron beam lithography (EBL) and *wet etched* using the dilute HCl etch with feature size ~40 nm achievable. This wet etching technique is suitable as there is no undercutting of the poly-methyl-methacrylate resist that would undermine the MnSb structure.

III. MEASUREMENTS

The anisotropic magnetoresistance (AMR) measurements were made using an 8 T magnet with a 1.7–295 K variable temperature insert. Magnetic fields could be applied in-plane or perpendicular to the substrate. Resistivity components ρ_{xx} and ρ_{xy} were measured using 100 nA ac currents at 33 Hz. The AMR signal was measured by sweeping the in-plane magnetic field either oriented along the Hall bar UEA (Uniaxial magnetic anisotropy Easy Axis) or at 90° to the Hall bar UHA (Uniaxial magnetic anisotropy Hard Axis) but still in-plane. Typical field ranges for the AMR measurements were ±2500 G (±0.25 T), compared to EA switching fields typically 500 to 1000 G. The EA direction is [1–10] and the HA direction is [110] on the GaAs(001) wafer (see Ref. 22) and is consistent with the measurements reported here. Device isolation was achieved by the built-in p–n junction with the n-type GaAs (001) and confirmed experimentally. A battery operated voltage pre-amplifier was used to reduce the random noise levels to <0.004% of the voltage signal associated with the AMR. Co-adding of simultaneous field sweep data was also used, with an optimum of ~10 sweeps. The longitudinal Magneto-optical Kerr effect (MOKE) signal was measured at 295 K in a 0.4 T electromagnet using a HeNe laser and linearly polarized optics.

Figures 2(a) and 2(b) show the longitudinal MOKE signal for a Mn-terminated wafer (device F) and an Sb-terminated wafer (device G), respectively, both having identical UA switching characteristics. Some monotonic background signal (a diamagnetic response) due to the finite doping levels can be seen, but this does not change the UMA interpretation or the switching field values.

For majority spin properties, there is no difference between Sb-terminated and Mn-terminated wafer surfaces, and this confirms what is already known about MnSb/GaAs (001). In Fig. 2(c), the normalized resistivity is plotted as a function of temperature. Ambient temperature resistivity is in the range of 90–400 $\mu\Omega$.cm (see Table I), and the resistivity reduces on cooling in a metallic behavior with no correlation to the surface termination. The resistivity ratio, i.e., R(295 K)/R(1.7 K), is 5.1 to 1.7 in the set of wafers with metallic behavior dominant.

Figure 3(a) shows the AMR signal from an Sb-terminated device (Wafer D) at discrete temperatures from 294 to 1.7 K. The field is oriented along the in-plane UEA, [1–10] direction for the GaAs substrate. The characteristics of an EA switching behavior are confirmed. The shaded area at ambient temperature shows the longitudinal MOKE signal with identical EA switching field, ~500 G. Figure 3(b) shows the same device with the field oriented in the orthogonal-in-plane UHA direction (the underlying GaAs [110] direction). The MOKE signal at 296 K shows a UHA characteristic as expected. The total AMR signal is 0.24% at 294 K for the Sb-terminated devices in comparison to the Mn-terminated devices that show an AMR signal <0.02% at 296 K.

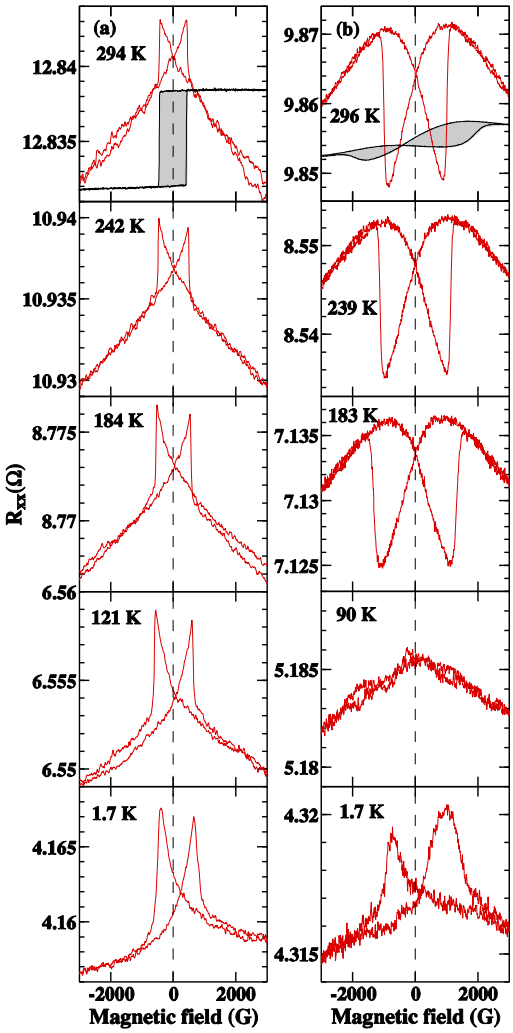

FIG. 3. (a) The magnetoresistance (R_{xx}) with (a) field parallel to current (B along the UMA easy axis) and (b) field perpendicular to current (B along the UMA HA) for device D (Sb-terminated) at discrete stabilized temperatures from 295 K down to 1.7 K. The shaded areas correspond to the longitudinal MOKE behavior at ambient temperature for the same applied field geometry.

When AMR is dominant, R_{xx} is given by

$$R_{xx} = R(\theta = 90^\circ) - \Delta R \times \cos^2\theta, \quad (1)$$

with $\Delta R = R(\theta = 90^\circ) - R(\theta = 0^\circ)$, where θ is the angle between the applied current and the applied in-plane magnetic field. ΔR can change sign, and this is observed in the anomalous temperature dependence of the AMR that is reported here.

In Fig. 4, we plot the size of the AMR as a function of temperature for the two orientations. The temperature dependence for the Mn-terminated devices (5 sets of data) are shown as the shaded region in Fig. 4. This quantity is close to ΔR from Eq. (1).

The AMR shows a strongly anomalous temperature dependence, for example, the size of the AMR signal reduces in magnitude

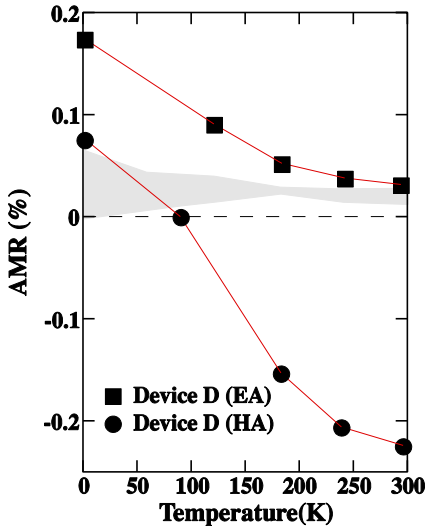

FIG. 4. The anisotropic magnetoresistance change as a function of temperature. The AMR signal is generated by sweeping the magnetic field, not rotating the field orientation with respect to the EA–HA directions. The gray shaded area is the data for the non Sb-capped devices A, B, C, E, and F. The polycrystalline sample device E shows a 0.02% AMR signal at 295 K and an AMR signal in the noise level (<0.004% of the background signal) at 1.7 K. Device D is the Sb-terminated surface.

along the UHA (Device D) but increases along the UEA. This shows the influence of a magneto-crystalline component. At 1.7 K, the UEA/UHA AMR signals look very similar [see Figs. 3(a) and 3(b) (the lowest panel)]. This is due to an additional magneto-crystalline term, i.e., it is the current along the [1–10] in-plane direction that determines the AMR in addition to a $\cos^2\theta$ term [see Eq. (1)], where θ is the angle between the applied field and the applied current. A polycrystalline wafer, device E, did not show an AMR signal; this was within the noise level <0.004% of the background R_{xx} signal at 1.7 K with no indication that a surface state was involved in the transport properties.

The (normal) Hall effect is linear in MnSb and is due to the majority spin properties although the high carrier density in these wafers means that the Hall voltages are small in comparison to those voltages arising from ρ_{xx}, and experimental mixing of the components can occur in non-ideal device geometries. Hall resistivity R_{xy} is dominated by the extraordinary Hall effect (EHE) for magnetic fields (B) <~2 T (see Fig. 5). The EHE contribution to ρ_{xy} is given by the following equation, with R_{xy} and ρ_{xy} variables interchangeable as the geometry correction factor is one for all geometries:

$$\rho_{xy} = R_H B + R_{EHE} M(B), \quad (2)$$

where R_H is the normal Hall constant, with $R_H = -r_H/e \times p$ and R_{EHE} is the extraordinary Hall constant. e is the fundamental unit of charge and p is the hole density. M is the magnetization, and r_H is the Hall correction factor that can be temperature dependent, 1.18 when scattering is limited by acoustic phonon scattering and 1.93 when the scattering is impurity dominated.

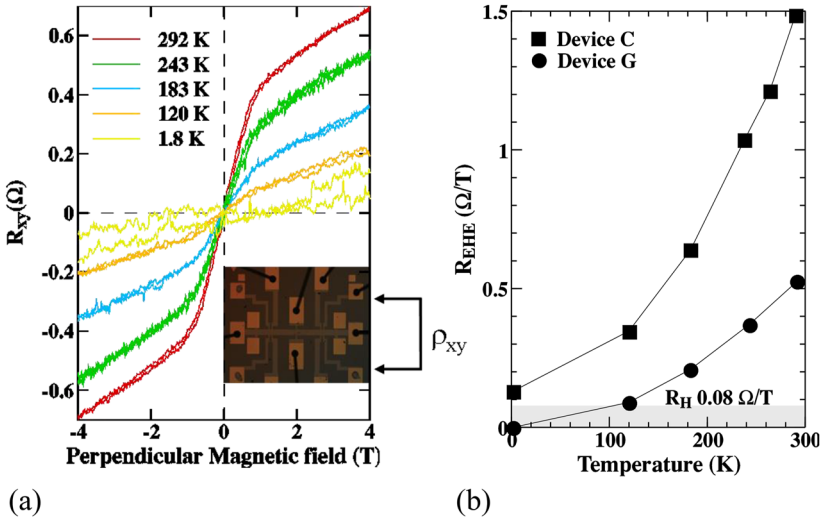

FIG. 5. (a) ρ_{xy} in device G (Sb-terminated) from 1.8 to 292 K. The inset shows the Hall contact geometry. (b) The extraordinary Hall coefficient (R_{EHE}) in device C (Mn-terminated) and device G (Sb-terminated). The ordinary Hall coefficient (R_H) is indicated in the shaded area, below which R_{EHE} cannot be determined.

Figure 5(a) shows R_{xy} for the Sb-terminated wafer G at discrete temperatures from 292 to 1.8 K. The normal Hall effect shows a carrier density of 0.5 to 2.0 × 10^{22} cm^{-3} from a Hall constant of ~0.08 Ω/T. This apparent variation is entirely due to the Hall correction factor (r_H) changing with temperature not a temperature dependent hole density. In the polycrystalline case,[23] an increase in the carrier density with temperature was attributed to delocalization of holes, but this mechanism is not operating in the MBE wafers as this process is likely to be thermally activated, of which there is no evidence here. The measured carrier densities show no difference in the Sb-terminated and the Mn-terminated devices as there is no surface layer for the majority spin carriers. However, the R_{EHE} constant shows a large difference, 1.5 Ω/T at 295 K for the Mn-terminated [Fig. 5(b)] compared to 0.5 Ω/T for the Sb-terminated devices. At 1.8 K, the EHE survives in the Mn-terminated devices, unlike the Sb-terminated devices; this could be due to the effect of the MnO or MnO_2 layer and is discussed further in Sec. IV. A stochastic noise signal develops in R_{xy} at low temperatures as the EHE is suppressed; this is clear in Fig. 5(a) and is not an experimental artifact.

IV. DISCUSSION

It has already been established that the structural and magnetic properties of MnSb are strongly influenced by the surface layer,[24–27] in particular, a bandgap in the minority spin band was predicted.[21,28] The measurements reported in this letter that are sensitive to the minority spin population suggest that the surface termination is important. The MOKE results confirm that the devices have predominantly uniaxial magnetic anisotropy although the underlying crystal structure is the niccolite-phase, which is not representative of a twofold symmetry. This is likely a surface reconstruction in the NiAs phase of Sb-terminated MnSb during MBE growth, as outlined in Ref. 20 where an additional contribution at the surface with a symmetry that is either Sb-rich (1 × 2) or Sb-poor *dis* (4 × 2) symmetry exists. The surface termination of the GaAs (001) starting substrate can also be influential in determining the bulk magnetic anisotropy of MnSb.[22]

The magnetoresistance signal in the HA direction (not an AMR signal) is typically ~1.0% ± 0.4% at 8 T, representative of majority spin band properties. There is no evidence of a conducting surface hole gas as there is no two-dimensional Shubnikov–de-Haas effect in ρ_{xx} up to 8 T at 1.7 K. There is no oscillatory structure in analog $d\rho_{xx}/dB$ and $d^2\rho_{xx}/dB^2$ signals from ultra-sensitive magnetic field modulation measurements up to 8 T with a 5 mT modulation field. However, the Sb-terminated devices show an enhanced AMR signal due to the influence of the minority spin band in providing a current carrying state at the surface.

An obvious question is as follows: Is the Sb-terminated surface just preventing MnO or MnO_2 forming and, hence influencing the AMR signal, perhaps reducing the measured signal? A simple etch test carried out on device D by removing the Sb-layer (with HCl) and then re-measuring as a function of temperature showed that etching the Sb-capped surface removes the large AMR signal (as seen in Fig. 4), resulting in a similar size AMR signal (~0.1% at 1.7 K in the EA direction) to the Mn-terminated surface. In the etched device, the majority spin properties change as well, indicating a resistivity ratio that is reduced from 3.1 to 2.1 after the HCl etch.

The anomalous temperature dependence of the AMR signal is also characteristic of that observed[30] in dilute magnetic semiconductors, such as $Ga_{1-x}Mn_xAs_{1-y}Sb_y$ alloys, where an additional magneto-crystalline anisotropy is reported. Magneto-crystalline AMR is also an important contribution in MnSb and demonstrates that highly ordered, single crystal growth is observed in the devices reported in this paper. In addition, MnAs exhibits a dominant crystalline AMR contribution, although this was not reported in the devices in Ref. 14. The extraordinary Hall effect is more prevalent in devices with the Mn-terminated surface. This suggests several possibilities: (1) the EHE signal is mainly coming from the bulk, (2) a

parallel conduction effect at the surface is suppressing the Hall voltage in the Sb-terminated wafers, or (3) the anomalous temperature dependence of the EHE is obscuring the role that the surface state provides in the minority spin band at the surface for the EHE. The normal Hall effect that is determined by the majority carrier density behaves in a similar fashion in all wafers, with a p-type Hall density between 5×10^{21} to 2×10^{22} cm^{-3}.

The coercive fields in MBE grown MnSb are in the region of ~500 G (0.05 T) as reported in Sec. III, making this a soft magnetic material and suitable for engineering the magnetic coercivity properties through lateral size modulation. Prototype devices were fabricated in a Mn-terminated MnSb device C and an Sb-terminated MnSb device G utilizing an EBL-defined nano-ring 200 nm in width. These devices showed evidence of a stable magnetic Vortex state[31] with future spintronic applications an exciting possibility. Further measurements will be forthcoming on the magnetic properties of a Vortex structure defined with a surface state in the minority spin bandgap.

V. CONCLUSIONS

The presence of spin-polarized surface states in half-metallic systems has been of interest for several years (see Refs. 21, 27, and 32) and was discussed in Secs. I and IV. In particular, the cubic phase of MnSb has conducting states in the minority spin bandgap at the surface,[32,33] and this property is critically dependent on the surface reconstruction during or after growth. Although the crystal structure of MBE grown MnSb is predominantly the niccolite-phase, we have presented evidence in this paper that the Sb-terminated surface has electrical properties that suggest conducting states exist in the minority spin bandgap. The electrical properties are determined nominally by the majority spin band behavior; however, anisotropic magnetoresistance sensitive to the minority spin band is <0.02% at 295 K in the bulk and has an enhanced signal, 0.24% in comparison to when the surface is Sb-terminated. An anomalous temperature dependence to the AMR and the EHE, particularly from a magneto-crystalline contribution in the MBE grown materials, does complicate this interpretation.[29,30]

Top-down processing of nano-structures can be achieved in niccolite MnSb using the dilute HCl-based etch developed in this work. This processing is compatible with EBL that can be engineered without undermining the electrical and magnetic properties of MnSb. This will provide devices for spin-injection of holes although this technology has to compete with higher efficiencies[34] available with magnesium oxide tunnel barrier structures for n-type spin-injection devices.

ACKNOWLEDGMENTS

This research program benefited from discussions with the Henry Royce Institute at the Cavendish Laboratory, University of Cambridge. We thank James D. Aldous and Chong Chen in this respect. The stability of the Vortex magnetic state was discussed with J. H. Lee and R. Mansell in the Thin Film Magnetism group at the Cavendish Laboratory.

AUTHOR DECLARATIONS

Conflict of Interest

The authors have no conflicts to disclose.

Author Contributions

S.N.H. developed device fabrication and measured the electrical and optical properties of the devices. C.W.B. and G.B. grew the MnSb wafers by MBE. I.F. and D.A.R. grew the as-capped GaAs substrate wafers. All the authors contributed to interpretation, discussion, and preparation of the publication.

S. N. Holmes: Conceptualization (equal); Data curation (equal); Formal analysis (equal); Investigation (equal); Methodology (equal); Project administration (equal); Resources (equal); Software (equal); Supervision (equal); Validation (equal); Visualization (equal); Writing – original draft (equal); Writing – review & editing (equal). **C. W. Burrows**: Conceptualization (equal); Data curation (equal); Formal analysis (equal); Investigation (equal); Validation (equal); Visualization (equal); Writing – original draft (equal); Writing – review & editing (equal). **G. R. Bell**: Conceptualization (equal); Data curation (equal); Formal analysis (equal); Funding acquisition (equal); Investigation (equal); Methodology (equal); Project administration (equal); Resources (equal); Validation (equal); Visualization (equal); Writing – review & editing (equal). **I. Farrer**: Conceptualization (equal); Data curation (equal); Formal analysis (equal); Investigation (equal); Methodology (equal); Resources (equal); Validation (equal); Visualization (equal); Writing – review & editing (equal). **D. A. Ritchie**: Conceptualization (equal); Data curation (equal); Formal analysis (equal); Funding acquisition (equal); Investigation (equal); Methodology (equal); Project administration (equal); Resources (equal); Supervision (equal); Validation (equal); Visualization (equal); Writing – review & editing (equal).

DATA AVAILABILITY

The data that support the findings of this study are openly available in Zenodo at https://zenodo.org/.

REFERENCES

[1] M. Z. Hasan and C. L. Kane, "*Colloquium*: Topological insulators," Rev. Mod. Phys. **82**, 3045 (2010).
[2] B. Bradlyn *et al.*, "Topological quantum chemistry," Nature **547**, 298 (2017).
[3] See https://topologicalquantumchemistry.org website for Topological Materials Database.
[4] W. Terui, H. Munekata, T. Hanna, and D. Yoshida, "MnSb-based spin LED with side-wall emission," Phys. Status Solidi C **8**, 396 (2011).
[5] T. Hanna, D. Yoshida, and H. Munekata, "Preparation characterization of MnSb–GaAs spin LED," J. Cryst. Growth **323**, 383 (2011).
[6] A. F. Panchula, C. Kaiser, A. Kellock, and S. P. StuartParkin, "Spin-polarization and magnetotransport of Mn–Sb alloys in magnetic tunnel junctions," Appl. Phys. Lett. **63**, 1812 (2003).
[7] M. Mizuguchi, H. Akinaga, K. Ono, and M. Oshima, "Fabrication and magnetotransport properties of nanoscaled MnSb dots," J. Appl. Phys. **87**, 5639 (2000).

[8]J. D. Aldous, C. W. Burrows, A. M. Sánchez, R. Beanland, I. Maskery, M. K. Bradley *et al.*, "Cubic MnSb: Epitaxial growth of a predicted room temperature half-metal," Phys. Rev. B **85**, 060403(R) (2012).
[9]G. R. Bell, C. W. Burrows, T. P. A. Hase, M. J. Ashwin, S. R. C. McMitchell, A. M. Sanchez, and J. D. Aldous, "Epitaxial growth of cubic MnSb on GaAs and InGaAs(111)," Spin **04**, 1440025 (2014).
[10]G. R. Bell, "Molecular beam epitaxy of transition metal monopnictides," in *Molecular Beam Epitaxy* (Elsevier, 2018), Chap. 1.
[11]P. J. Mousley, C. W. Burrows, M. J. Ashwin, A. M. Sánchez, V. K. Lazarov, and G. R. Bell, "Growth and characterisation of MnSb(0001)/InGaAs(111)A epitaxial films," J. Cryst. Growth **498**, 391 (2018).
[12]C. Dempsey, J. Dong, H. Inbar, A. Engel, A. Goswami, Y.-H. Chang, S. Nishihaya, P. Vlad, and C. Palmstrom, "Molecular beam epitaxy growth of ferromagnetic MnSb on InGaSb: Characterization of orientation, interfaces, and magnetic properties," in APS March Meeting 2022, Abstract id.W12.002, Bibcode 2022APS.MARW12002D, 2022.
[13]C. W. Burrows, A. Dobbie, M. Myronov, T. P. A. Hase, S. B. Wilkins, M. Walker, J. J. Mudd, I. Maskery, M. R. Lees, C. F. McConville, D. R. Leadley, and G. R. Bell, "Heteroepitaxial growth of ferromagnetic MnSb(0001) films on Ge/Si(111) virtual substrates," Cryst. Growth Des. **13**, 4923 (2013).
[14]E. D. Fraser, S. Hegde, L. Schweidenback, A. H. Russ, A. Petrou, H. Luo, and G. Kioseoglou, "Efficient electron spin injection in MnAs-based spin-light-emitting-diodes up to room temperature," Appl. Phys. Lett. **97**, 041103 (2010).
[15]S. Jahangir, F. Doğan, H. Kum, A. Manchon, and P. Bhattacharya, "Spin diffusion in bulk GaN measured with MnAs spin injector," Phys. Rev. B **86**, 035315 (2012).
[16]N. Nishizawa and H. Munekata, "Thickness dependence of magnetic anisotropy in MnSb epitaxial layers," J. Cryst. Growth **378**, 418 (2013).
[17]X. Chen, M. Na, M. Cheon, S. Wang, H. Luo, B. D. McCombe, X. Liu, Y. Sasaki, T. Wojtowicz, J. K. Furdyna, S. J. Potashnik, and P. Schiffer, "Above-room-temperature ferromagnetism in GaSb/Mn digital alloys," Appl. Phys. Lett. **81**, 511 (2002).
[18]S. A. Hatfield, J. D. Aldous, and G. R. Bell, "Stoichiometry, contamination and microstructure of MnSb(0001) surfaces," Appl. Surf. Sci. **255**, 3567 (2009).
[19]J. D. Aldous, C. W. Burrows, I. Maskery, M. S. Brewer, T. P. A. Hase, J. A. Duffy, M. R. Lees, C. Sánchez-Hanke, T. Decoster, W. Theis, A. Quesada, A. K. Schmid, and G. R. Bell, "Depth-dependent magnetism in epitaxial MnSb thin films: Effects of surface passivation and cleaning," J. Phys.: Condens. Matter **24**, 146002 (2012).
[20]S. A. Hatfield and G. R. Bell, "Mapping the surface reconstructions of MnSb(0001) and," Surf. Sci. **601**, 5368 (2007).
[21]S. J. Jenkins, "Tilted elliptical Dirac cones at a half-metal surface," Phys. Rev. B **82**, 020403(R) (2010).
[22]H. Akinaga, S. Miyanishi, W. Van Roy, J. De Boeck, and G. Borghs, "Influence of GaAs (001) surface termination on the in-plane magnetic anisotropies of MnSb epitaxial films," Appl. Phys. Lett. **73**, 3285 (1998).
[23]L. N. Oveshnikov, A. B. Granovsky, A. B. Davydov, A. V. Bogach, A. M. Kharlamova, A. I. Ril, and B. A. Aronzon, "Magnetic and magnetotransport properties of MnSb polycrystals near equatomic composition," J. Magn. Magn. Mater. **563**, 169873 (2022).
[24]J. I. Lee and S. C. Hong, "Surface electronic structure and magnetism of NiAs structured MnAs(0001) and MnSb(0001)," J. Appl. Phys. **101**, 09G502 (2007).
[25]O. Rader, M. Ležaić, S. Blügel, A. Fujimori, A. Kimura, N. Kamakura, A. Kakizaki, S. Miyanishi, and H. Akinaga, "Spin-polarized surface state of MnSb(0001)," New J. Phys. **7**, 111 (2005).
[26]K. Lawniczak-Jablonska *et al.*, "Structural and magnetic properties of the molecular beam epitaxy grown MnSb layers on GaAs substrates," J. Appl. Phys. **106**, 083524 (2009).
[27]S. J. Jenkins and D. A. King, "Minority metallic surface states of a half-metallic ferrimagnet," Surf. Sci. **494**, L793 (2001).
[28]G. Y. Gao and K. L. Yao, "Bulk and surface half-metallicity: Metastable zinc-blende TiSb," J. Appl. Phys. **112**, 023712 (2012).
[29]H. Akinaga, Y. Suzuki, K. Tanaka, K. Ando, and T. Katayama, "Crystal-orientation dependence on magnetic circular dichroism spectra of MnSb epitaxial film," Appl. Phys. Lett. **67**, 141 (1995).
[30]B. Howells, M. Wang, K. W. Edmonds, P. Wadley, R. P. Campion, A. W. Rushforth, C. T. Foxon, and B. L. Gallagher, "Crystalline anisotropic magnetoresistance in quaternary ferromagnetic semiconductor (Ga,Mn)(As,Sb)," Appl. Phys. Lett. **102**, 052407 (2013).
[31]S. N. Holmes, J.-H. Lee, B. Hong, M. D. Mascaro, D. Anderson, G. A. C. Jones, C. A. Ross, and C. H. W. Barnes, "Magnetic vortex stability in $Ni_{80}Fe_{20}$ split rings," J. Appl. Phys. **113**, 044508 (2013).
[32]S. J. Jenkins, "Ternary half-metallics and related binary compounds: Stoichiometry, surface states, and spin," Phys. Rev. B **70**, 245401 (2004).
[33]S. Mollet and S. J. Jenkins, "Surface states and surface stability in half-metallic systems: The cases of zinc-blende-structure MnSb {111}A, {111}B and {001}," J. Phys.: Condens. Matter **19**, 315214 (2007).
[34]X. Jiang, R. Wang, R. M. Shelby, R. Macfarlane, S. R. Bank, J. S. Harris, and S. S. P. Parkin, "Highly spin-polarized room-temperature tunnel injector for semiconductor spintronics using MgO(100)," Phys. Rev. Lett. **94**, 056601 (2005).